nanomaterials

MDPI

Review

Ultrasmall-in-Nano: Why Size Matters

Ryan D. Mellor and Ijeoma F. Uchegbu *

School of Pharmacy, University College London (UCL), 29–39 Brunswick Square, London WC1N 1AX, UK; ryan.mellor.16@ucl.ac.uk
* Correspondence: ijeoma.uchegbu@ucl.ac.uk

Abstract: Gold nanoparticles (AuNPs) are continuing to gain popularity in the field of nanotechnology. New methods are continuously being developed to tune the particles' physicochemical properties, resulting in control over their biological fate and applicability to in vivo diagnostics and therapy. This review focuses on the effects of varying particle size on optical properties, opsonization, cellular internalization, renal clearance, biodistribution, tumor accumulation, and toxicity. We review the common methods of synthesizing ultrasmall AuNPs, as well as the emerging constructs termed ultrasmall-in-nano—an approach which promises to provide the desirable properties from both ends of the AuNP size range. We review the various applications and outcomes of ultrasmall-in-nano constructs in vitro and in vivo.

Keywords: ultrasmall-in-nano; gold nanoparticles; clearance; biodistribution; tumor accumulation; toxicity

1. Introduction

Colloidal gold is the subject of ever-growing interest in the field of nanotechnology. This is due to its versatility and tunability in terms of size, shape, and surface chemistry. With a rigorous understanding of the properties of gold nanoparticles (AuNPs) comes the ability to exploit them for a plethora of therapeutic and diagnostic applications.

Almost any material will display three distinct size-dependent ranges of properties, in their atomic-, nano-, and bulk-scale [1]. Thus, most materials can feasibly exist as a 'nanomaterial' between 1 and 1000 nanometers; however, to be of any practical use, its properties must be precisely and reproducibly manipulated at scale and, under this criteria, AuNPs excel. Various methods (chemical and physical) have been developed to accurately control AuNP's size (from 1 to 330 nm), shape (spheres, rods, stars, plates, cubes, cages, and shells), surface chemistry, and optical-electronic properties. Furthermore, AuNPs are inert, non-toxic, and can be made to be stable in a range of solvents and pH values, properties which are desirable from a biological standpoint [2].

With progress into the tunability of almost every aspect of AuNPs comes the opportunity to investigate how varying each one of these properties independently will affect the physicochemical properties and biological outcome of the particles. One of the easiest and most effective ways to control the properties of AuNPs is by varying the size. There are advantages and disadvantages for AuNPs in both the ultrasmall (<5 nm) and the nano (5–1000 nm) size range, in terms of the optical properties, cellular uptake, opsonization, toxicity, biodistribution, tumor accumulation, and excretability. This work will outline some of the methods implemented to synthesize ultrasmall AuNPs, the trends observed with varying AuNP size, and finally, the approaches and applications of ultrasmall-in-nano—a new construct which is able to combine the advantages from both ends of the size range.

Citation: Mellor, R.D.; Uchegbu, I.F. Ultrasmall-in-Nano: Why Size Matters. *Nanomaterials* **2022**, *12*, 2476. https://doi.org/10.3390/nano12142476

Academic Editor: Rodolphe Antoine

Received: 20 June 2022
Accepted: 13 July 2022
Published: 19 July 2022

2. Effects of Varying Size

2.1. Effect on Optical Properties

Varying the size of AuNPs is one of the most straightforward and efficient ways to alter the optical properties and enhance scattering [3]. AuNPs exhibit surface plasmon resonance (SPR), meaning that, at a particular range of wavelengths, dependent on the particles' size and shape, they will display increased absorbance. This is a distinctly nano property, not observed at either the atomic or bulk scale of gold [4]. This SPR band can be exploited to create diagnostic techniques such as surfaced enhanced Raman spectroscopy (SERS) [5] and spatially offset Raman spectroscopy (SORS) [6], and for therapeutic techniques including photothermal therapy (PTT) [7] and photodynamic therapy (PDT) [8]. For diagnostic and therapeutic applications, the SPR band should reside in a region known as the phototherapeutic window—650–850 nm, a range of low absorbance by biomolecules in human tissue, resulting in the high depth penetration of the incident laser light [9]. Unfortunately, particles which exhibit this SPR band tend to be in the size range of 100–200 nm [10], a size that would not be sufficiently excreted by the kidneys.

Generally, larger particles will have a more redshifted SPR peak compared to their smaller counterparts [11]. Spheres in the ultrasmall size range (~5 nm) will exhibit SPR peaks in the range of 515–520 nm and this will bathochromically shift to over 570 nm with an increasing particle diameter beyond 100 nm [12]. This bathochromic shift is accompanied by a broadening of the resonance [3,11].

It is also reported that SERS intensity increases with particle size [11], this is of huge significance for theranostic applications of AuNPs as a stronger SERS intensity results in particles which can be detected at lower concentrations and greater depth. Further investigation is required to determine the interplay between particle size, laser wavelength, and SERS intensity [11].

2.2. Effect on Opsonization

Nanoparticles, upon introduction to the bloodstream, collide with proteins, some of which will bind to the particle, forming a biological identity known as a protein corona. A fraction of these proteins will be opsonins, such as complement proteins [13] and antibodies [14], which tag the particle for uptake by phagocytes and elimination from the body. This is a vital aspect of the immune system and it is responsible for the removal of, among other things, pathogens, diseased cells and protein aggregates [15]; however, this phagocytosis leads to the undesirable reduced circulation time of nanoparticles. One of the most successful approaches to avoid opsonization is by altering the nanoparticle's surface chemistry, for example, by PEGylation [16,17]; however, the particle's size can also have a dramatic effect.

It has been shown that, for nanoparticles and proteins of similar sizes, their attraction resulting from van der Walls potential scales with the particles radii [18]. Therefore, it follows that larger particles will experience a greater degree of opsonization, as has been shown experimentally for particles with diameters of 7–22 nm [19]. The increased opsonization can be explained in part by the increased surface area; however, this is not a complete explanation, as it has been shown that the density of adsorbed proteins also increases [20]. This trend would not be expected to hold indefinitely, since there reaches a point where, due to the decreasing curvature, the particle's surface is indistinguishable from being flat from the perspective of a protein. Indeed, that size limit has been shown to be on the order of 50 nm, after which the protein binding diminishes with increasing size [21].

2.3. Effect on Cellular Internalization

It is usually desirable to either suppress or promote cellular internalization, depending on the theranostic application. Suppression is generally advantageous if the application does not require activity within the cell, for example, imaging or PTT; this allows efficient elimination of the nanoparticle after it has served its purpose [22]. Conversely, the promo-

tion of cellular internalization also has its applications, for example, the delivery of cargo which acts intracellularly. However, when a system is designed to promote initialization, efforts should be made to minimize systemic toxicity arising from non-specific internalization, and this may be achieved by coating the particle with a targeting moiety [23].

Nanoparticles rely heavily on receptor-mediated endocytosis for cellular internalization [24,25]. This results in the rate of internalization, with regards to nanoparticle size, being governed by two opposing phenomena. Larger particles can bind to many cell-surface receptors simultaneously, which leads a decrease in the Gibbs free energy, resulting in the membrane wrapping around the particle. On the one hand, a smaller particle is only able to interact with a few receptors at a time; this means that there is no risk of a localized receptor shortage which would act to reduce the overall rate of particle uptake. Similarly, larger particles require a greater surface area of the cell membrane to envelope the particle, whereas smaller particles require a greater surface curvature of the cell membrane, neither of which are favorable due to either kinetics or energetics, respectively. Several studies, both theoretical [25–27] and experimental [28,29], have found the sweet spot for efficient internalization to be around 25–50 nm. However, this range is heavily dependent on the particles' surface chemistry [30] and cell-line [31] being tested. More generally, 10–100 nm is considered the optimal range for favoring internalization, where particles outside of this range will suffer from one of the aforementioned phenomena.

2.4. Effect on Renal Clearance

The renal clearance of injected agents is desirable to avoid hazards resulting from the accumulation and/or decomposition of said agents. In order for efficient renal clearance, particles must poses a hydrodynamic diameter below that of the kidney filtration threshold (KFT) of ~5.5 nm [32,33], a limit set by the size of the glomerular pores that filter blood plasma. Particles of up to 8 nm may be filtered by the kidneys provided so that the particle surface is positively charged; this is due to favorable interactions with the filtration barrier, which are not present for neutral or negatively charged particles [34]. Particles that are not able to be filtered by the kidneys will rely on the slower hepatobiliary pathway for clearance, if they are to be excreted at all.

It is noteworthy that there exists a Goldilocks zone for the size of renally clearable particles of approximately 1–5 nm; this is assumed to be due to fact that particles below 1 nm can enter the ~1 nm pores of the glomerular glycocalyx. This is evidenced by the exponential decrease in rate of glomerular filtration with increasing particle size for atomically precise AuNPs below 1 nm, where the size is inferred from the particles' mass as determined by electrospray ionization mass spectroscopy [35].

Multiple studies [36,37] have compared particles within the size range 1–5 nm to particles larger than 5 nm and the findings are in almost unanimous agreement. That is, larger (>5 nm) particles show low to undetectable levels in the urine as they cannot pass through the glomerular pores, and significant levels accumulating in the liver and excreted via the hepatobiliary pathway. Meanwhile, smaller (<5 nm) particles show higher rates of excretion via both the renal and hepatobiliary pathways, where more than 50% of the injected dose (%ID) is cleared in hours [38], rather than weeks [39] to months [40], for larger particles. Notably, it is the hydrodynamic diameter, and not that of the solid core, which determines the fate of a nanoparticle. This is nicely demonstrated by varying the molecular weight, and therefore the thickness, of a PEG coating while maintaining a gold core size of 2.5 nm; the <5 nm hydrodynamic diameter particles showed preferential renal clearance, while the >5 nm hydrodynamic diameter particles showed a decreased rate that would be expected of larger particles [41]. The correlation of size vs. rate of excretion has been shown to be exponential in nature [42], where particles of 2, 6, and 13 nm demonstrated renal clearance efficiencies of 50, 4, and 0.5%, respectively, 24 h post-injection.

2.5. Effect on Biodistribution

The biodistribution of nanoparticles is heavily impacted by not only the particle size, but also the shape and surface chemistry; therefore, it is important to bear in mind that the trends observed when changing any one of these parameters can be enhanced or countered by changing one of the others. That said, all else being equal, there are significant correlations between biodistribution and size. Figure 1 summarizes some of the ways in which biodistribution is affected by the particles' properties.

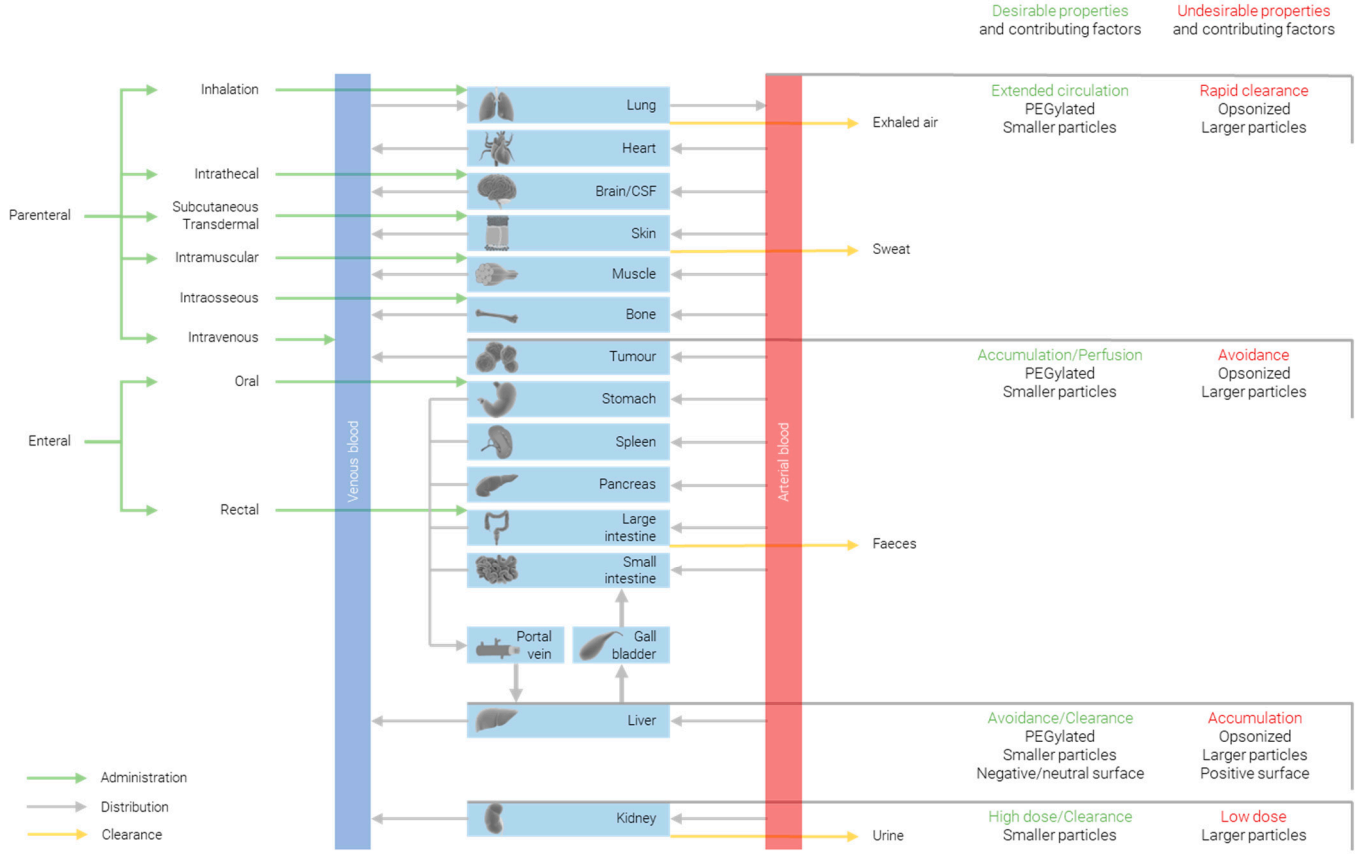

Figure 1. Approaches for modulating biodistribution of nanoparticles.

Generally, it is shown that smaller particles exhibit a more widespread distribution than larger ones. One study compared the biodistribution of 10, 50, 100, and 250 nm particles 24 h after intravenous injection [43]. They found detectable levels of the largest particles (100 and 250 nm) in the blood, liver, and spleen, with negligible quantities (0.1 %ID) in the kidneys; smaller 50 nm particles were further detected in the lungs and heart; and only the smallest 10 nm particles were detected in the remaining tissues in the testis, thymus, and brain, with a larger quantity (1 %ID) present in the kidneys. Across all sizes tested, the highest organ accumulation was found to be in the liver. A similar study, comparing 15, 50, 100, and 200 nm particles, found almost identical results, with the exception that 50 nm particles were additionally detected in the brain [44]; this may be attributed to the different animal models and AuNP preparations used in the two studies [45].

2.6. Effect on Tumor Accumulation

For any cancer theranostic, it is necessary to achieve some degree of targeting. In the case of diagnostic applications, a construct must be able to accumulate at the tumor in order to distinguish it from healthy tissue and identify the tumor. For therapy, tumor accumulation allows tissue damage to be focused on the diseased tissue to the greatest extent possible, maximizing efficacy and minimizing adverse side effects.

One popular approach is to functionalize the surface of constructs with tumor-targeting antibodies, aptamers, peptides, or small molecules; however, this is outside of the scope of this review; we refer the reader to the review "Active targeting of gold nanoparticles as cancer therapeutics" [46] for an overview of the subject. Within the scope is the opportunity for size-based passive targeting. Nanoparticles need to fall within a particular size rage (40–400 nm [47]) in order to take advantage of the enhanced permeability and retention (EPR) effect. The EPR effect leads to passive preferential accumulation in tumor tissue due to a combination of the leaky vasculature, compared to the continuous endothelial junctions of healthy tissue, and reduced lymphatic drainage that would normally help to carry away cytotoxic compounds [48]. For passive targeting to be effective, the therapeutic must remain in circulation for as long as possible. To accomplish an extended half-life, the NPs may be functionalized to tune the particle's size, surface charge, hydrophobicity, and surface chemistry in order to reduce the renal and phagocytic clearance [49].

Size plays a key role in a particle's ability to preferentially accumulate at a tumor. Small particles show more widespread distribution amongst all tissues, both healthy and diseased; they can diffuse more freely into the tumor from the vasculature [50], but this also means that they diffuse out again at a greater rate. Larger particles, close to or exceeding 1 µm, are unable to pass through the tumor fenestrae, with pores in the order of a few hundred nanometers [51]; they are also less able to diffuse into solid tumors, which may not be problematic if the intended application is diagnostic, where locating at the tumor boundary is sufficient.

As discussed in the previous section, smaller particles exhibit extended circulation times and this tends to lead to increased tumor accumulation compared to larger particles; ultrasmall AuNPs have been shown to have a particularly high tumor accumulation when compared to >10 nm AuNPs [52].

2.7. Effect on Toxicity

The correlation between size and toxicity of AuNPs is not easy to discern from the literature, due to inconsistent synthesis methods, capping ligands, cell/animal models, dosages, and routes of administration [53]. Toxicity has been reported for ultrasmall (<2 nm) AuNPs, and when the bare gold surface is accessible [54]. The toxicity of ultrasmall AuNPs may be attributed to the more widespread biodistribution and longer circulation times when compared to larger particles which rapidly accumulate in the liver.

Most studies report AuNPs as being non-toxic, and where toxicity is observed, it is generally attributed to physicochemical properties derived from the capping ligand as opposed to the gold core itself.

On the other hand, one study looked at citrate-capped particles ranging from 3 to 100 nm, performing an in vitro MTT ((3-(4,5-dimethylthiazol-2-yl)-2,5-diphenyltetrazolium bromide) assay against Hela cells to assess the particles and found no cytotoxicity for any size at any concentration (up to 0.4 mM). The study also determined the average lifespan (L_{50}) of BALB/c mice dosed intraperitoneally with 8 mg/kg/week for each particle size and no toxicity or lethality was observed for small particles (3, and 5 nm) or for large particles (50, and 100 nm); however, intermediate particles (8, 12, 17, and 37 nm) all showed an L_{50} of less than 21 days. The authors suggest that the zone of toxicity is attributed to particles being small enough to enter cells but large enough to avoid initiating a specific immune response [55].

3. Methods to Synthesize Ultrasmall AuNPs

A plethora of methods have been developed to precisely control the size, shape, and surface chemistry of AuNPs. These range from green synthesis methods, where the AuNPs are produced either by microorganisms or plant extracts [56–58], to physical methods such as laser ablation [59–61], thermal decomposition [62,63], and mechanical milling [64], and finally, chemical synthesis methods. Chemical synthesis methods are perhaps the most widely employed methods, owing to the vast array of physicochemical properties which

can be achieved and the specificity with which they can be obtained. Many approaches exist to chemically synthesize AuNPs; however, they all proceed via essentially the same steps (Figure 2):

- **Reduction** of Au^{3+}—afforded by a gold salt, usually $HAuCl_4$—to atomic Au^0; this process is rapid and continues until the concentration of gold atoms in solution reaches supersaturation.
- **Nucleation** of gold atoms into gold clusters; the number of nucleation sites determines the number concentration of AuNPs, i.e., for a fixed mass concentration more nucleation events results in smaller particles and vice versa.
- **Growth** via coalescence of gold clusters and diffusion of remaining soluble gold atoms onto the surface of gold agglomerates.

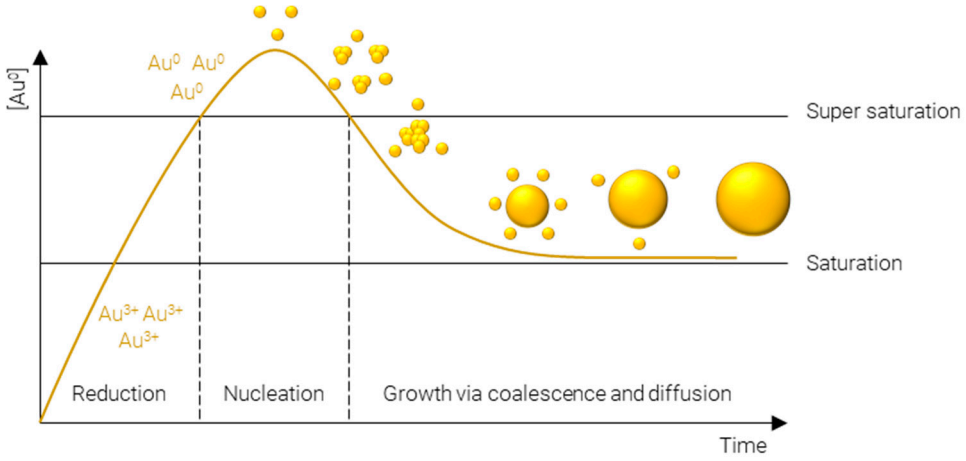

Figure 2. LaMer model of metal nanoparticle formation.

The following sections will outline some of the most common methods used to synthesize ultrasmall AuNPs; they have been divided into the four main methods used in the literature—Turkevich/Frens, reduction by sodium borohydride, Brust–Schiffrin, and seeded growth. Where reagent names have been abbreviated, the meaning can be found in Table 1.

Table 1. Abbreviations for reagents use in AuNP synthesis.

Abbreviation	Meaning
BDAC	Benzyldimethylhexadecylammonium chloride
CTAB	Cetyltrimethylammonium bromide
CTAC	Cetyltrimethylammonium chloride
GSH	Glutathione
$HAuCl_4$	Chloroauric acid
HQL	8-hydroxyquinoline
MPA	Mercaptopropionic acid
$NaBH_4$	Sodium borohydride
NaI	Sodium iodide
ODA	Octadecylamine
PVP	Polyvinylpyrrolidone
TOAB	Tetraoctylammonium bromide

Turkevich/Frens (Figure 3A) synthesis is the classical method of producing AuNPs. It was one of the first systematic approaches to the size-controlled synthesis of AuNPs and is still popular today, owing largely to its simplicity and reliability. The method was pioneered Turkevich et al. in 1951 [65], producing 15–24 nm AuNPs, and later refined by Frens in 1973 [66], extending the size range to 16–147 nm. In this synthesis, citrate is used as both reducing agent and capping agent; however, citrate is not a strong enough

reducing agent to rapidly generate atomic gold at room temperature; therefore, the synthesis is carried out at elevated temperature, typically boiling. The AuNPs' size is controlled predominantly by the ratio of citrate:Au, where more citrate results in more rapid nucleation and, subsequently, smaller particles. Particle size and distribution may also be controlled by pH [67], temperature [68], and order of reagent addition [69]. While AuNPs with an average diameter of 4 nm have been reportedly synthesized by the Turkevich method with minor modifications [70], it is far more common for particles to be larger than 10 nm in diameter.

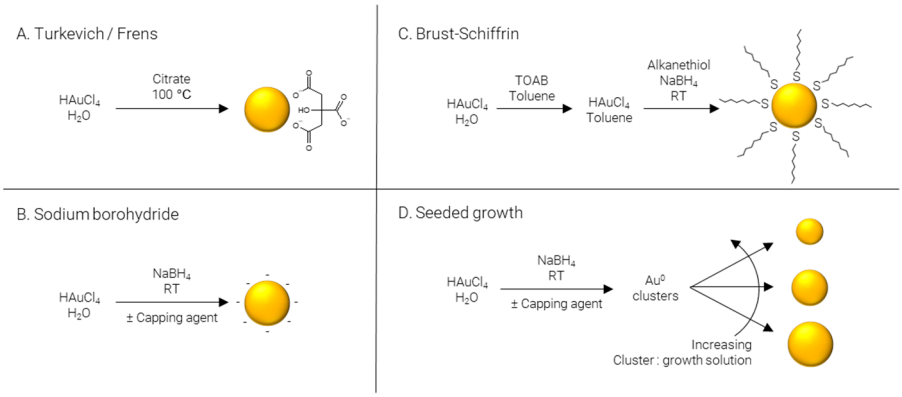

Figure 3. Methods of AuNP synthesis.

Sodium borohydride (Figure 3B) is often implemented as a strong reducing agent in the synthesis of AuNPs enabling the reaction to be performed at room temperature and allowing for rapid nucleation and formation of smaller AuNPs, frequently sub 5 nm. Like the Turkevich method, citrate may be included; however, when $NaBH_4$ is used as a reducing agent, citrate severs solely as a capping agent [71]. Alternatively, citrate can be replaced by other hydrophilic capping agents such as alginate [72] or chitosan [73]. The synthesis may also be performed in non-polar solvents such as chloroform, implementing hydrophobic capping agents such as CTAB [74] and ODA [75,76]. Finally, capping agents may be omitted entirely to produce "bare" AuNPs [77].

Brust–Schiffrin (Figure 3C) synthesis is a two-phase approach to produce alkanethiol-capped AuNPs which are soluble in hydrophobic solvents. TOAB is employed to transfer $AuCl_4^-$ from the aqueous phase to an organic phase, typically toluene; $NaBH_4$ is used to reduce the gold salt in the presence of a capping agent, traditionally an alkanethiol. The capping agent first used, and still commonly used today, is the alkanethiol dodecanethiol [78]; however, this may be replaced with other alkanethiols such as pentanethiol [79] or hexanethiol [80], surfactants such as CTAB or CTAC [81], or even ionizable molecules for the synthesis of water soluble AuNPs, for example via the use of MPA [82].

Seeded growth (Figure 3D) is synthetic process of first producing Au^0 clusters, often via $NaBH_4$, although Turkevich/Frens particles may also be used as seeds, which are then introduced as presynthesized nuclei into a growth solution. Essentially, the particle number concentration of the resulting solution can be finely controlled by varying the number of nuclei introduced and the final particle size is regulated by the gold concentration in the growth solution. This approach is not particularly well suited to the formation of ultrasmall AuNPs and is more commonly employed for the preparation of particles over a large size range [83,84]. As well as being applicable over large size ranges, seeded growth is also capable of producing a wide variety of shapes by using different shape directing agents, such as CTAC for spheres [85] and cubes [86], CTAC/NaI for triangles [87], CTAB/CTAC/HQL for bipyramids/javelins [88], PVP for stars [89], and BDAC/CTAB for rods [90].

The methods outlined in the previous sections are summarized in Table 2.

Table 2. Methods of AuNP Synthesis. Focusing mainly on ultrasmall spheres, with several prominent examples of methods for synthesizing larger or non-spherical particles.

Method of Synthesis	Size Range	Shape	Surface Chemistry	Polarity	Solvent	Ref.
Turkevich	15–24 nm	Sphere	Citrate	Hydrophilic	H_2O	[65]
Frens	16–147 nm	Sphere	Citrate	Hydrophilic	H_2O	[66]
Turkevich/Frens	4 nm	Sphere	Citrate	Hydrophilic	H_2O	[70]
Sodium borohydride	3–5 nm	Sphere	Citrate	Hydrophilic	H_2O	[71]
Sodium borohydride	3.3–12	Sphere	Alginate	Hydrophilic	H_2O	[72]
Sodium borohydride	3.5–14 nm	Sphere	Chitosan	Hydrophilic	H_2O	[73]
Sodium borohydride	3–14 nm	Sphere	CTAB	Hydrophobic	$CHCl_3$	[74]
Sodium borohydride	4.7 nm	Sphere	ODA	Hydrophobic	$CHCl_3$	[75]
Sodium borohydride	3 nm	Sphere	ODA	Hydrophobic	$CHCl_3$	[76]
Sodium borohydride	3–5 nm	Sphere	Bare	Hydrophilic	H_2O	[77]
Turkevich/Frenz—modified	3.6–13 nm	Sphere	Citrate/tannic acid	Hydrophilic	H_2O	[91]
Turkevich/Frenz—modified	3.5–15 nm	Sphere	PDEAEM	Hydrophilic	H_2O	[92]
Turkevich/Frenz—modified	2–330 nm	Sphere	Citrate	Hydrophilic	H_2O	[93]
Brust-Schiffrin	1–3 nm	Sphere	Dodecanethiol	Hydrophobic	Toluene	[78]
Brust-Schiffrin	5 nm	Sphere	Pentanethiol	Hydrophobic	Toluene	[79]
Brust-Schiffrin	2 nm	Sphere	Hexanethiol	Hydrophobic	Toluene	[80]
Brust-Schiffrin	10 nm	Sphere	CTAB/CTAC	Hydrophobic	Toluene	[81]
Brust-Schiffrin	3 nm	Sphere	MPA	Variable	Toluene/H_2O	[82]
Seeded growth	8.4–180.5 nm	Sphere	Citrate	Hydrophilic	H_2O	[83]
Seeded growth	15–300 nm	Sphere	Citrate	Hydrophilic	H_2O	[84]
Seeded growth	5–150	Sphere	CTAC	Hydrophilic	H_2O	[85]
Seeded growth	60 nm	Triangle	CTAC/NaI	Hydrophilic	H_2O	[87]
Seeded growth	76 nm	Cube	CTAC	Hydrophilic	H_2O	[86]
Seeded growth	40–300 nm	Bipyramid/Javelin	CTAB/CTAC/HQL	Hydrophilic	H_2O	[88]
Seeded growth	45–116 nm	Star	PVP	Hydrophilic	DMF	[89]
Seeded growth	10–100 nm	Rod	BDAC/CTAB	Hydrophilic	H_2O	[90]
Other—GSH reduction	2.5 nm	Sphere	GSH	Hydrophilic	H_2O	[94]
Other—GSH reduction	2.3 nm	Sphere	GSH/cysteamine	Hydrophilic	H_2O	[95]
Other—HEPES reduction	23 nm	Star	HEPES	Hydrophilic	H_2O	[96]
Other—TBAB reduction	2–7 nm	Sphere	Oleylamine	Hydrophobic	DCM	[97]
Other—TBAB reduction	3–10 nm	Sphere	Oleylamine	Hydrophobic	Hexane	[98]
Other—thermal reduction	2 nm	Sphere	PEG	Hydrophilic	H_2O	[99]
Other—mechanochemical	1–4 nm	Sphere	Various	Various	None	[64]

4. Ultrasmall-in-Nano—Approaches and Applications

One approach which has been gaining popularity in the past few years is referred to as an ultrasmall-in-nano [30] construct: 'ultrasmall' represents the sub-5 nm gold cores, and 'nano' represents the 100–500 nm clusters of said AuNPs. While gold itself is inert and biocompatible, problems arise when considering persistence of the gold in the body [30]. The body's main mechanism for excretion of compounds from circulation, specifically, via the renal pathway, is not efficient at removing particles larger than 5 nm in diameter [100]. This is mainly due to the functional pore size of the glomerular capillary wall of 4.5–5 nm [101] and larger particles will instead rely on elimination via the hepatobiliary pathway. Consequently, particles below this threshold are desirable to avoid the potential retention of gold in the body. However, several desirable properties result from particles only in the 100–500 nm range. These properties include increased circulation times [102], superior accumulation in tumor tissue due to the enhanced permeability and retention effect [103], and specifically in the case of AuNPs strong absorbance in the phototherapeutic window [104]. A work around for these diametrically opposed concepts is to have a system which can be converted from the latter to the former after its function has been served, i.e., from larger (100–500 nm) nanoparticles to ultrasmall (sub-5 nm) particles.

To display the desired optical properties, specifically, a bathochromic shift in absorbance upon clustering, the ultrasmall particles must come into proximity of one another. The effect of interparticle electromagnetic coupling is proportional to the inverse of inter-

particle distance [105], suggesting that the most prominent bathochromic shift is obtained when the ultrasmall particles are as close as possible without touching to avoid irreversible fusion, as would be observed with other aggregation methods, for example, upon the addition of glucosamine phosphate to small AuNPs [106].

Many approaches have been reported for forming ultrasmall-in-nano constructs; while they all follow what is essentially the same schematic, depicted in Figure 4, and have some common characteristics, they differ in the approach used to cluster the ultrasmalls and in the application of the nano construct. Some of these approaches are outlined in the following sections and summarized in Table 3.

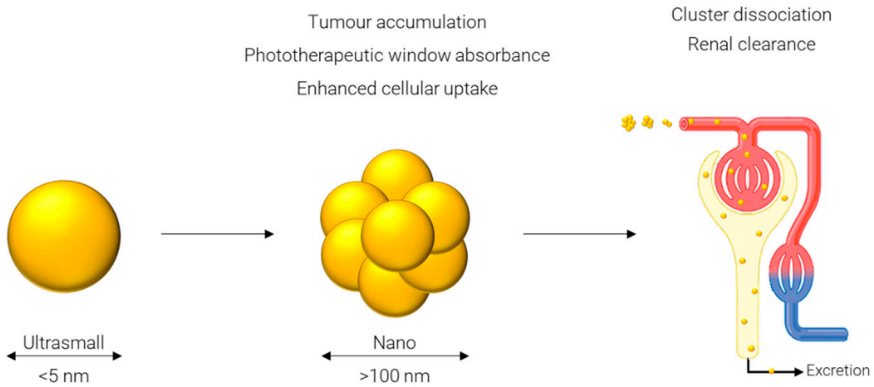

Figure 4. Generalized principle of the ultrasmall-in-nano approach.

Table 3. Methods of generating ultrasmall-in-nano constructs.

Ultrasmall (Surface Chemistry, and Size)	Nano (Clustering Principle, and Size)	SPR	Reversible	Refs.
ODA 4.67 ± 1.74 nm	Crosslinking with EGBMA 254–278 nm	710 nm	Yes	[75]
NA 2–8 nm	Coating of DSPC: cholesterol liposomes 100–120 nm	760 nm	Yes	[107]
Tannic acid and/or citrate 3, 5, and 13 nm	Single stranded DNA-coated AuNPs + complementary linker 50–150 nm	Nr	Yes	[108]
PSS ~3 nm (varies with article)	Ionic interactions with PL ~100 nm (varies with article)	530 nm	Yes	[109–114]
AcetalDextran-pMBA-AuNPs 2.1 ± 0.5 nm	Encapsulation in PEG-PCL 111.1 ± 38 nm	Nr	Nr	[115]
11-MUA or GSH 2–5 nm	Encapsulation in PCPP 40–500 nm	>650 nm	Yes	[116]
GSH ~2 nm	Encapsulation in PAA HCl 120 nm	Nr	Nr	[117]
Citrate/lysine 4.1 ± 0.8 nm	Interaction with PLA(2K)-PEG(10K)-PLA(2K) 83.0 ± 4.6 nm	Broad, NIR absorbance	Yes	[118]
NA 6.1 ± 1.8 nm	Self-assembly with PCL-PHEMA and $PMEO_2MA$ 300 nm	800 nm	Nr	[119]

Nr: Nor reported.

4.1. Approaches to Clustering

4.1.1. Small Molecule Crosslinking

Mellor et al. [75] showed that using a labile dithiol molecule—ethylene glycol bis-mercaptoacetate (EGBMA)—they were able cluster octadecylamine (ODA) AuNPs (sub-5 nm) and demonstrated that, under physiological conditions, the clusters can revert

to ultrasmall AuNPs. The nano constructs exhibited strong absorbance in the phototherapeutic window and were labelled with a Raman reporter, allowing for specific detection in a biological matrix, demonstrating its feasibility for future theranostic applications.

4.1.2. Coating of Liposomes

Rengan et al. [107] prepared a formulation that can be described as ultrasmall-on-nano, by first forming 1,2-distearoyl-sn-glycero-3-phosphocholine (DSPC): cholesterol liposomes in the nano range, and subsequently coating them with ultrasmall AuNPs (2–8 nm). They demonstrate the ability of these particles, following intratumoral injection, to kill cancer cells using PTT with complete ablation of the tumor mass following 750 nm laser illumination. The particles are shown to be degraded in hepatocytes and cleared through the hepato-biliary and renal routes. On days 1, 7, and 14, the %ID detected in the liver was 52%, 9.8%, and 3%, respectively, and in the kidney was 2.7%, 0.25%, and 0.22%, respectively. This demonstrated a significant reduction in gold levels in just 14 days, and the authors hypothesized that renal excretion would be increased when the constructs are subjected to both photothermal and enzymatic degradation.

4.1.3. DNA Assembly

Chou et al. [108] designed a core-satellite architecture whereby AuNPs (13 nm cores, and 3 or 5 nm satellites) coated with thiolated, single-stranded DNA were then assembled using complementary sequence linker DNA. They demonstrated that, by careful selection of the DNA sequence and capping ligand, they could tune a number of properties: the constructs' ability to encapsulate small molecules, their propensity for cellular uptake, elimination, and tumor-targeting. In addition, in this study, gold content in urine was quantified 48 h after systemic injection of cores, satellites, and core-satellite constructs. They found the highest levels of renal excretion for the smallest particles tested—15 %ID for 3 nm satellites with a 1 kDa PEG coating—and decreasing levels with increasing particle size or PEG molecular weight. Similarly, for the core-satellite constructs, they found that the urine levels were proportional to the size of the satellite tested, and lower than that of the respective satellite alone. This finding suggests, as would be expected, that only the satellites are being excreted and not the 13 nm cores.

4.1.4. Encapsulation/Ionic Interaction

Voliani and their team demonstrated, in multiple articles [109–114], their ultrasmall-in-nano construct, referred to as 'passion fruit'-like, formed by ionic interaction between poly(l-lysine) (PL) and poly(sodium 4-styrene sulfonate) (PSS)-coated ultrasmall AuNPs (~3 nm). They studied their tumor-targeting ability following modification with a peptide [109]; biocompatibility and excretion in murine models where they showed excretion from both renal and biliary pathways [110]; pharmacokinetics following inhalation [111], showing accumulation in the lungs, translocation to secondary organs, and almost complete excretion within 10 days; and the suitability of their ultrasmall-in-nano construct for PTT applications [114]. The researchers monitored the biodistribution and excretion for 10 days following intravenous injection through the tail vein. They observed that the gold concentration in the liver decreased over the course of time, and that gold was detected in both urine and faces for the duration of the experiment for a cumulative excretion of ~16 %ID in 10 days.

Higbee-Dempsey et al. [115] prepared ultrasmall p-MBA-AuNPs coated with thiolated dextran (2.1 nm); the dextran was made to be hydrophobic by the covalent incorporation of acetyl groups. The hydrophobic AcetalDextran-pMBA-AuNPs were mixed with poly(ethylene glycol)-block-poly(ε-caprolactone) (PEG-PCL), resulting in micellization and dense packing of the ultrasmall cores. Acetyl groups were shown to be cleaved in an acidic environment, resulting in a hydrophilic polymer, demicellization, and dispersion of gold cores. The group showed clearance of gold from mice organs over 3 months, following a single bolus injection via the tail vein. They report that levels in the liver and spleen

reduced by 86% and 72%, respectively, and that gold is detected in urine and faeces at decreasing levels over the time course; however, the reported levels represent samples collected on the day of sacrifice, and do not represent the cumulative excretions between time points.

Cheheltani et al. [116] encapsulated ultrasmall GSH-coated AuNPs (2–5 nm) in a biodegradable poly di(carboxylatophenoxy)phosphazene (PCPP) polymer; they were able to control the size of the particles, and therefore, the position of the SPR peak in the NIR region, by varying the amount of polyethylene glycol-polylysine block co-polymer in the formulation. They demonstrate the potential of these constructs as computed tomography (CT) and photoacoustic (PA) imaging contrast agents both in vitro and in vivo. They also demonstrate the ability of the clusters to degrade upon incubation in serum.

Yahia-Ammar et al. [117] first synthesized ultrasmall GSH-coated AuNPs (~2 nm); these particles were then encapsulated by the addition of poly(allyl amine hydrochloride) (PAA HCl) polymer. They show that the clustered particles exhibit enhanced fluorescence compared to the ultrasmall particles, with quantum yield increasing from 7 to 25%. They also demonstrated the increased cellular uptake of these particles and the application of this to enhanced cellular delivery of both peptides and antibodies.

Tam et al. [118] clustered ultrasmall lysine/citrate-capped AuNPs (4.1 nm) via ionic interaction with biodegradable triblock copolymer of polylactic acid and polyethylene glycol (PLA(2K)-PEG(10K)-PLA(2K)). Upon cluster formation, the absorbance maximum shifted from 520 nm into the NIR region with a fairly constant absorbance of 700 to 900 nm. Limited degradation was observed after 4 weeks at neutral pH, whereas almost total degradation was observed after just 1 week at pH 5, a finding attributed to the stability of PLA at neutral pH. Nanocluster degradation was confirmed in vitro by TEM and scattering spectra from hyperspectral images of treated and untreated murine macrophage cells over 168 h.

Deng et al. [119] worked with 6.1 nm particles, which is on the upper limit of what may be considered ultrasmall, as acknowledged by the researchers; however, the approach may be transferable to smaller particles to ensure excretability. Their system is based on the self-assembly of AuNPs within a novel comb-like amphipathic polymer composed of hydrophobic poly(ε-caprolactone)/poly(2-hydroxyethyl methacrylate) (PCL-PHEMA) and hydrophilic poly(2-(2-methoxyethoxy) ethyl methacrylate) ($PMEO_2MA$). The group tested the potential of the particles for PTT by exposing solutions of various concentrations to 808 nm NIR laser at a power density of 1.5 W cm^{-2}; at the highest concentration (0.4 mg mL^{-1}), they observed heating up to 71 °C after laser irradiation for 5 min. They also loaded DOX into the particles, which was released following laser irradiation to demonstrate the combined chemotherapeutic and phototherapeutic abilities of the construct. The constructs were shown to be suitable as contrast agents for both CT and PAT imaging. The researchers monitored the levels of the gold in the tumor, vital organs (heart, liver, spleen, lung, and kidney), and vital metabolic products (bile, urine, and faces) for 7 days following intratumoral injection. They found that levels in the tumor decreased over the course of time; the levels in the vital organs increased until day 2, but then had decreased by day 7, and the levels in metabolic products increased over the course of time. The increasing renal excretion over the course of the experiment, with 4 %ID detected in the urine on day 7, suggests disassembly of the constructs back to ultrasmall AuNPs, and that 6 nm AuNPs are still renally excreted, if only to a lower extent than smaller particles.

4.2. Accomplishments of Ultrasmall-in-Nano Constructs

It is clear that ultrasmall-in-nano provides a viable route to produce constructs with the properties of particles larger than their constituent cores; in various studies, they have been shown to have absorbance in the phototherapeutic window [75,107,116,118,119], to be SERS active [75], to be suitable as PTT agents [107,114,119], and to function as PA and CT contrast agents [116], amongst other key characteristics.

What has also been demonstrated, to a lesser extent, is the excretion of ultrasmall particles following administration of nano constructs. Where in vivo studies have been performed to monitor retention and/or excretion, they have demonstrated quite varied results, suggesting that the excretion rate is highly dependent on the approach to clustering, as well as the size of the ultrasmall particle. Rengan et al. [103] showed fairly quick decrease in levels of gold detected in the liver of 52% to 3%ID over 14 days, whereas Higbee-Dempsey et al. [115] reported ~85% elimination from the liver over three months. It is promising that studies such as those performed by Chou et al. [108] demonstrated that the rate of excretion of ultrasmall-in-nano constructs is proportional to the sizes of the constituent ultrasmall particles. This highlights the necessity for the entirety of the construct to be comprised of ultrasmall particles, as the 13 nm cores do not appear to have been excreted.

Several studies, where excretion has not yet been demonstrated experimentally, have reported that their ultrasmall-in-nano constructs are able to liberate ultrasmall particles [75,117,119]. This, combined with the data of the aforementioned in vivo studies, suggests that there are several emerging constructs with the potential to deliver the capabilities of nanoparticles, while retaining the excretable nature of ultrasmall particles.

5. Conclusions and Future Perspectives

Optical properties, opsonization, cellular internalization, renal clearance, biodistribution, tumor accumulation, and toxicity all display size-dependent relationships with gold nanoparticles. In some regards, smaller particles are favored, for example for increased renal clearance; in others its larger particles, such as to display strong absorbance in the phototherapeutic window. Clearly, it is not possible to have a single static construct which displays all these properties; however, ultrasmall-in-nano promises a dynamic structure to provide the advantages of the small and the large.

Where the properties of the larger particles are disadvantageous, work-arounds have been proposed which usually entail the modification of the particles' surface, for example, PEGylation to reduce the propensity for opsonization, or conjugation to a targeting moiety to increase tumor accumulation.

It is noteworthy that the examples of ultrasmall-in-nano reviewed here were all from the last decade or so; this emphasizes how novel this work is and the interest its subject matter has gained in a relatively short time.

Ultrasmall-in-nano constructs have already been shown to deliver a lot of what the concept promises, from phototherapeutic absorbance and SERS activity to declustering and excretion. Future works will likely focus on combining many of these properties into a single construct and demonstrating complete excretion in a reasonable timeframe.

Author Contributions: Writing—original draft preparation, R.D.M.; writing—review and editing, R.D.M. and I.F.U. All authors have read and agreed to the published version of the manuscript.

Funding: This research was funded by UK Engineering and Physical Sciences Research Council, grant number EP/R020965/1.

Institutional Review Board Statement: Not applicable.

Informed Consent Statement: Not applicable.

Data Availability Statement: Not applicable.

Conflicts of Interest: The authors declare no conflict of interest.

References

1. Roduner, E. Size matters: Why nanomaterials are different. *Chem. Soc. Rev.* **2006**, *35*, 583–592. [CrossRef] [PubMed]
2. Chan, W.C.W. (Ed.) *Bio-Applications of Nanoparticles*; Advances in Experimental Medicine and Biology; Springer: Berlin/Heidelberg, Germany; Landes Bioscience: Austin, TX, USA, 2007; ISBN 978-0-387-76712-3.
3. Lee, K.-S.; El-Sayed, M.A. Dependence of the Enhanced Optical Scattering Efficiency Relative to That of Absorption for Gold Metal Nanorods on Aspect Ratio, Size, End-Cap Shape, and Medium Refractive Index. *J. Phys. Chem. B* **2005**, *109*, 20331–20338. [CrossRef] [PubMed]
4. Mohapatra, S.; Ranjan, S.; Dasgupta, N.; Kumar, R.; Thomas, S. *Characterization and Biology of Nanomaterials for Drug Delivery: Nanoscience and Nanotechnology in Drug Delivery*; Elsevier: Amsterdam, The Netherlands, 2018; ISBN 978-0-12-814032-1.
5. Langer, J.; Jimenez de Aberasturi, D.; Aizpurua, J.; Alvarez-Puebla, R.A.; Auguié, B.; Baumberg, J.J.; Bazan, G.C.; Bell, S.E.J.; Boisen, A.; Brolo, A.G.; et al. Present and Future of Surface-Enhanced Raman Scattering. *ACS Nano* **2020**, *14*, 28–117. [CrossRef] [PubMed]
6. Mosca, S.; Conti, C.; Stone, N.; Matousek, P. Spatially offset Raman spectroscopy. *Nat. Rev. Methods Primer* **2021**, *1*, 21. [CrossRef]
7. Wei, W.; Zhang, X.; Zhang, S.; Wei, G.; Su, Z. Biomedical and bioactive engineered nanomaterials for targeted tumor photothermal therapy: A review. *Mater. Sci. Eng. C* **2019**, *104*, 109891. [CrossRef]
8. Chen, J.; Fan, T.; Xie, Z.; Zeng, Q.; Xue, P.; Zheng, T.; Chen, Y.; Luo, X.; Zhang, H. Advances in nanomaterials for photodynamic therapy applications: Status and challenges. *Biomaterials* **2020**, *237*, 119827. [CrossRef]
9. Diwu, Z.; William Lown, J. Phototherapeutic potential of alternative photosensitizers to porphyrins. *Pharmacol. Ther.* **1994**, *63*, 1–35. [CrossRef]
10. Niu, J.; Zhu, T.; Liu, Z. One-step seed-mediated growth of 30–150 nm quasispherical gold nanoparticles with 2-mercaptosuccinic acid as a new reducing agent. *Nanotechnology* **2007**, *18*, 325607. [CrossRef]
11. Njoki, P.N.; Lim, I.-I.S.; Mott, D.; Park, H.-Y.; Khan, B.; Mishra, S.; Sujakumar, R.; Luo, J.; Zhong, C.-J. Size Correlation of Optical and Spectroscopic Properties for Gold Nanoparticles. *J. Phys. Chem. C* **2007**, *111*, 14664–14669. [CrossRef]
12. Haiss, W.; Thanh, N.T.K.; Aveyard, J.; Fernig, D.G. Determination of Size and Concentration of Gold Nanoparticles from UV−Vis Spectra. *Anal. Chem.* **2007**, *79*, 4215–4221. [CrossRef]
13. Merle, N.S.; Noé, R.; Halbwachs-Mecarelli, L.; Fremeaux-Bacchi, V.; Roumenina, L.T. Complement System Part II: Role in Immunity. *Front. Immunol.* **2015**, *6*, 257. [CrossRef] [PubMed]
14. Chiu, M.L.; Goulet, D.R.; Teplyakov, A.; Gilliland, G.L. Antibody Structure and Function: The Basis for Engineering Therapeutics. *Antibodies* **2019**, *8*, 55. [CrossRef] [PubMed]
15. Cockram, T.O.J.; Dundee, J.M.; Popescu, A.S.; Brown, G.C. The Phagocytic Code Regulating Phagocytosis of Mammalian Cells. *Front. Immunol.* **2021**, *12*, 629979. [CrossRef] [PubMed]
16. Petros, R.A.; DeSimone, J.M. Strategies in the design of nanoparticles for therapeutic applications. *Nat. Rev. Drug Discov.* **2010**, *9*, 615–627. [CrossRef] [PubMed]
17. Yoo, J.-W.; Chambers, E.; Mitragotri, S. Factors that Control the Circulation Time of Nanoparticles in Blood: Challenges, Solutions and Future Prospects. *Curr. Pharm. Des.* **2010**, *16*, 2298–2307. [CrossRef]
18. Lane, L.A.; Qian, X.; Smith, A.M.; Nie, S. Physical Chemistry of Nanomedicine: Understanding the Complex Behaviors of Nanoparticles in Vivo. *Annu. Rev. Phys. Chem.* **2015**, *66*, 521–547. [CrossRef]
19. Deng, Z.J.; Liang, M.; Toth, I.; Monteiro, M.J.; Minchin, R.F. Molecular Interaction of Poly(acrylic acid) Gold Nanoparticles with Human Fibrinogen. *ACS Nano* **2012**, *6*, 8962–8969. [CrossRef]
20. Kaur, K.; Forrest, J.A. Influence of particle size on the binding activity of proteins adsorbed onto gold nanoparticles. *Langmuir* **2012**, *28*, 2736–2744. [CrossRef]
21. Lacerda, S.H.D.P.; Park, J.J.; Meuse, C.; Pristinski, D.; Becker, M.L.; Karim, A.; Douglas, J.F. Interaction of Gold Nanoparticles with Common Human Blood Proteins. *ACS Nano* **2010**, *4*, 365–379. [CrossRef]
22. Yu, M.; Zheng, J. Clearance Pathways and Tumor Targeting of Imaging Nanoparticles. *ACS Nano* **2015**, *9*, 6655–6674. [CrossRef]
23. Ruoslahti, E.; Bhatia, S.N.; Sailor, M.J. Targeting of drugs and nanoparticles to tumors. *J. Cell Biol.* **2010**, *188*, 759–768. [CrossRef] [PubMed]
24. Jiang, W.; Kim, B.Y.S.; Rutka, J.T.; Chan, W.C.W. Nanoparticle-mediated cellular response is size-dependent. *Nat. Nanotechnol.* **2008**, *3*, 145–150. [CrossRef]
25. Gao, H.; Shi, W.; Freund, L.B. Mechanics of receptor-mediated endocytosis. *Proc. Natl. Acad. Sci. USA* **2005**, *102*, 9469–9474. [CrossRef] [PubMed]
26. Yuan, H.; Li, J.; Bao, G.; Zhang, S. Variable nanoparticle-cell adhesion strength regulates cellular uptake. *Phys. Rev. Lett.* **2010**, *105*, 138101. [CrossRef] [PubMed]
27. Decuzzi, P.; Ferrari, M. The role of specific and non-specific interactions in receptor-mediated endocytosis of nanoparticles. *Biomaterials* **2007**, *28*, 2915–2922. [CrossRef]
28. Chithrani, B.D.; Ghazani, A.A.; Chan, W.C.W. Determining the Size and Shape Dependence of Gold Nanoparticle Uptake into Mammalian Cells. *Nano Lett.* **2006**, *6*, 662–668. [CrossRef] [PubMed]
29. Liu, X.; Huang, N.; Li, H.; Jin, Q.; Ji, J. Surface and size effects on cell interaction of gold nanoparticles with both phagocytic and nonphagocytic cells. *Langmuir* **2013**, *29*, 9138–9148. [CrossRef]

30. Li, B.; Lane, L.A. Probing the biological obstacles of nanomedicine with gold nanoparticles. *Wiley Interdiscip. Rev. Nanomed. Nanobiotechnol.* **2019**, *11*, e1542. [CrossRef]
31. Albanese, A.; Tang, P.S.; Chan, W.C.W. The Effect of Nanoparticle Size, Shape, and Surface Chemistry on Biological Systems. *Annu. Rev. Biomed. Eng.* **2012**, *14*, 1–16. [CrossRef]
32. Longmire, M.; Choyke, P.L.; Kobayashi, H. Clearance Properties of Nano-sized Particles and Molecules as Imaging Agents: Considerations and Caveats. *Nanomedicine* **2008**, *3*, 703–717. [CrossRef]
33. Liu, J.; Yu, M.; Zhou, C.; Zheng, J. Renal clearable inorganic nanoparticles: A new frontier of bionanotechnology. *Mater. Today* **2013**, *16*, 477–486. [CrossRef]
34. Adhipandito, C.F.; Cheung, S.-H.; Lin, Y.-H.; Wu, S.-H. Atypical Renal Clearance of Nanoparticles Larger Than the Kidney Filtration Threshold. *Int. J. Mol. Sci.* **2021**, *22*, 11182. [CrossRef] [PubMed]
35. Du, B.; Jiang, X.; Das, A.; Zhou, Q.; Yu, M.; Jin, R.; Zheng, J. Glomerular Barrier Behaves As an Atomically Precise Bandpass Filter in a Sub-nanometre Regime. *Nat. Nanotechnol.* **2017**, *12*, 1096–1102. [CrossRef] [PubMed]
36. Semmler-Behnke, M.; Kreyling, W.G.; Lipka, J.; Fertsch, S.; Wenk, A.; Takenaka, S.; Schmid, G.; Brandau, W. Biodistribution of 1.4- and 18-nm gold particles in rats. *Small* **2008**, *4*, 2108–2111. [CrossRef]
37. Balogh, L.; Nigavekar, S.S.; Nair, B.M.; Lesniak, W.; Zhang, C.; Sung, L.Y.; Kariapper, M.S.T.; El-Jawahri, A.; Llanes, M.; Bolton, B.; et al. Significant effect of size on the in vivo biodistribution of gold composite nanodevices in mouse tumor models. *Nanomed. Nanotechnol. Biol. Med.* **2007**, *3*, 281–296. [CrossRef]
38. Hainfeld, J.F.; Slatkin, D.N.; Focella, T.M.; Smilowitz, H.M. Gold nanoparticles: A new X-ray contrast agent. *Br. J. Radiol.* **2006**, *79*, 248–253. [CrossRef]
39. Renaud, G.; Hamilton, R.L.; Havel, R.J. Hepatic metabolism of colloidal gold-low-density lipoprotein complexes in the rat: Evidence for bulk excretion of lysosomal contents into bile. *Hepatology* **1989**, *9*, 380–392. [CrossRef]
40. Sadauskas, E.; Danscher, G.; Stoltenberg, M.; Vogel, U.; Larsen, A.; Wallin, H. Protracted elimination of gold nanoparticles from mouse liver. *Nanomed. Nanotechnol. Biol. Med.* **2009**, *5*, 162–169. [CrossRef]
41. Zhao, Y.; Sultan, D.; Detering, L.; Luehmann, H.; Liu, Y. Facile synthesis, pharmacokinetic and systemic clearance evaluation, and positron emission tomography cancer imaging of ^{64}Cu–Au alloy nanoclusters. *Nanoscale* **2014**, *6*, 13501–13509. [CrossRef]
42. Zhou, C.; Long, M.; Qin, Y.; Sun, X.; Zheng, J. Luminescent Gold Nanoparticles with Efficient Renal Clearance. *Angew. Chem. Int. Ed.* **2011**, *50*, 3168–3172. [CrossRef]
43. De Jong, W.H.; Hagens, W.I.; Krystek, P.; Burger, M.C.; Sips, A.J.A.M.; Geertsma, R.E. Particle size-dependent organ distribution of gold nanoparticles after intravenous administration. *Biomaterials* **2008**, *29*, 1912–1919. [CrossRef] [PubMed]
44. Sonavane, G.; Tomoda, K.; Makino, K. Biodistribution of colloidal gold nanoparticles after intravenous administration: Effect of particle size. *Colloids Surf. B Biointerfaces* **2008**, *66*, 274–280. [CrossRef] [PubMed]
45. Khlebtsov, N.; Dykman, L. Biodistribution and toxicity of engineered gold nanoparticles: A review of in vitro and in vivo studies. *Chem. Soc. Rev.* **2011**, *40*, 1647–1671. [CrossRef] [PubMed]
46. Goddard, Z.R.; Marín, M.J.; Russell, D.A.; Searcey, M. Active targeting of gold nanoparticles as cancer therapeutics. *Chem. Soc. Rev.* **2020**, *49*, 8774–8789. [CrossRef] [PubMed]
47. Subhan, M.A.; Yalamarty, S.S.K.; Filipczak, N.; Parveen, F.; Torchilin, V.P. Recent Advances in Tumor Targeting via EPR Effect for Cancer Treatment. *J. Pers. Med.* **2021**, *11*, 571. [CrossRef]
48. Greish, K. Enhanced Permeability and Retention (EPR) Effect for Anticancer Nanomedicine Drug Targeting. In *Cancer Nanotechnology: Methods and Protocols*; Grobmyer, S.R., Moudgil, B.M., Eds.; Methods in Molecular Biology; Humana Press: Totowa, NJ, USA, 2010; pp. 25–37. ISBN 978-1-60761-609-2.
49. Blanco, E.; Shen, H.; Ferrari, M. Principles of nanoparticle design for overcoming biological barriers to drug delivery. *Nat. Biotechnol.* **2015**, *33*, 941–951. [CrossRef]
50. Perrault, S.D.; Walkey, C.; Jennings, T.; Fischer, H.C.; Chan, W.C.W. Mediating Tumor Targeting Efficiency of Nanoparticles Through Design. *Nano Lett.* **2009**, *9*, 1909–1915. [CrossRef]
51. Jain, R.K.; Stylianopoulos, T. Delivering nanomedicine to solid tumors. *Nat. Rev. Clin. Oncol.* **2010**, *7*, 653–664. [CrossRef]
52. Huang, K.; Ma, H.; Liu, J.; Huo, S.; Kumar, A.; Wei, T.; Zhang, X.; Jin, S.; Gan, Y.; Wang, P.C.; et al. Size-dependent localization and penetration of ultrasmall gold nanoparticles in cancer cells, multicellular spheroids, and tumors in vivo. *ACS Nano* **2012**, *6*, 4483–4493. [CrossRef]
53. Sani, A.; Cao, C.; Cui, D. Toxicity of gold nanoparticles (AuNPs): A review. *Biochem. Biophys. Rep.* **2021**, *26*, 100991. [CrossRef]
54. Schmid, G.; Kreyling, W.G.; Simon, U. Toxic effects and biodistribution of ultrasmall gold nanoparticles. *Arch. Toxicol.* **2017**, *91*, 3011–3037. [CrossRef] [PubMed]
55. Chen, Y.-S.; Hung, Y.-C.; Liau, I.; Huang, G.S. Assessment of the In Vivo Toxicity of Gold Nanoparticles. *Nanoscale Res. Lett.* **2009**, *4*, 858–864. [CrossRef] [PubMed]
56. Bharadwaj, K.K.; Rabha, B.; Pati, S.; Sarkar, T.; Choudhury, B.K.; Barman, A.; Bhattacharjya, D.; Srivastava, A.; Baishya, D.; Edinur, H.A.; et al. Green Synthesis of Gold Nanoparticles Using Plant Extracts as Beneficial Prospect for Cancer Theranostics. *Molecules* **2021**, *26*, 6389. [CrossRef] [PubMed]
57. Lee, K.X.; Shameli, K.; Miyake, M.; Kuwano, N.; Khairudin, N.B.B.A.; Mohamad, S.E.B.; Yew, Y.P. Green Synthesis of Gold Nanoparticles Using Aqueous Extract of Garcinia mangostana Fruit Peels. *J. Nanomater.* **2016**, *2016*, e8489094. [CrossRef]

58. Esther, J.; Sridevi, V. Synthesis and characterization of chitosan-stabilized gold nanoparticles through a facile and green approach. *Gold Bull.* **2017**, *50*, 1–5. [CrossRef]
59. Mafuné, F.; Kohno, J.; Takeda, Y.; Kondow, T.; Sawabe, H. Formation of Gold Nanoparticles by Laser Ablation in Aqueous Solution of Surfactant. *J. Phys. Chem. B* **2001**, *105*, 5114–5120. [CrossRef]
60. Lévy, A.; De Anda Villa, M.; Laurens, G.; Blanchet, V.; Bozek, J.; Gaudin, J.; Lamour, E.; Macé, S.; Mignon, P.; Milosavljević, A.R.; et al. Surface Chemistry of Gold Nanoparticles Produced by Laser Ablation in Pure and Saline Water. *Langmuir* **2021**, *37*, 5783–5794. [CrossRef]
61. Amendola, V.; Polizzi, S.; Meneghetti, M. Laser Ablation Synthesis of Gold Nanoparticles in Organic Solvents. *J. Phys. Chem. B* **2006**, *110*, 7232–7237. [CrossRef]
62. Cho, S.P.; Jang, S.; Jo, H.N.; Lee, S.A.; Bae, S.; Lee, S.H.; Hwang, J.; Joh, H.I.; Wang, G.; Kim, T.W. One step synthesis of Au nanoparticle-cyclized polyacrylonitrile composite films and their use in organic nano-floating gate memory applications. *J. Mater. Chem. C* **2016**, *4*, 1511–1516. [CrossRef]
63. Bakrania, S.D.; Rathore, G.K.; Wooldridge, M.S. An investigation of the thermal decomposition of gold acetate. *J. Therm. Anal. Calorim.* **2009**, *95*, 117–122. [CrossRef]
64. Rak, M.J.; Saadé, N.K.; Friščić, T.; Moores, A. Mechanosynthesis of ultra-small monodisperse amine-stabilized gold nanoparticles with controllable size. *Green Chem.* **2014**, *16*, 86–89. [CrossRef]
65. Turkevich, J.; Stevenson, P.C.; Hillier, J. A study of the nucleation and growth processes in the synthesis of colloidal gold. *Discuss. Faraday Soc.* **1951**, *11*, 55–75. [CrossRef]
66. Frens, G. Controlled Nucleation for the Regulation of the Particle Size in Monodisperse Gold Suspensions. *Nat. Phys. Sci.* **1973**, *241*, 20–22. [CrossRef]
67. Tyagi, H.; Kushwaha, A.; Kumar, A.; Aslam, M. A Facile pH Controlled Citrate-Based Reduction Method for Gold Nanoparticle Synthesis at Room Temperature. *Nanoscale Res. Lett.* **2016**, *11*, 362. [CrossRef]
68. Tran, M.; DePenning, R.; Turner, M.; Padalkar, S. Effect of citrate ratio and temperature on gold nanoparticle size and morphology. *Mater. Res. Express* **2016**, *3*, 105027. [CrossRef]
69. Ojea-Jiménez, I.; Bastús, N.G.; Puntes, V. Influence of the Sequence of the Reagents Addition in the Citrate-Mediated Synthesis of Gold Nanoparticles. *J. Phys. Chem. C* **2011**, *115*, 15752–15757. [CrossRef]
70. Yang, Y.; Shi, J.; Chen, H.; Dai, S.; Liu, Y. Enhanced off-resonance optical nonlinearities of Au@CdS core-shell nanoparticles embedded in $BaTiO_3$ thin films. *Chem. Phys. Lett.* **2003**, *370*, 1–6. [CrossRef]
71. Al-Johani, H.; Abou-Hamad, E.; Jedidi, A.; Widdifield, C.M.; Viger-Gravel, J.; Sangaru, S.S.; Gajan, D.; Anjum, D.H.; Ould-Chikh, S.; Hedhili, M.N.; et al. The structure and binding mode of citrate in the stabilization of gold nanoparticles. *Nat. Chem.* **2017**, *9*, 890–895. [CrossRef]
72. Beishenaliev, A.; Faruqu, F.N.; Leo, B.F.; Lit, L.C.; Loke, Y.L.; Chang, C.-C.; Teo, Y.Y.; Chik, Z.; Foo, Y.Y.; Chung, L.Y.; et al. Facile synthesis of biocompatible sub-5 nm alginate-stabilised gold nanoparticles with sonosensitising properties. *Colloids Surf. A Physicochem. Eng. Asp.* **2021**, *627*, 127141. [CrossRef]
73. Abrica-González, P.; Zamora-Justo, J.A.; Sotelo-López, A.; Vázquez-Martínez, G.R.; Balderas-López, J.A.; Muñoz-Diosdado, A.; Ibáñez-Hernández, M. Gold nanoparticles with chitosan, N-acylated chitosan, and chitosan oligosaccharide as DNA carriers. *Nanoscale Res. Lett.* **2019**, *14*, 258. [CrossRef] [PubMed]
74. Fan, C.; Jiang, L. Preparation of Hydrophobic Nanometer Gold Particles and Their Optical Absorption in Chloroform. *Langmuir* **1997**, *13*, 3059–3062. [CrossRef]
75. Mellor, R.D.; Schätzlein, A.G.; Uchegbu, I.F. Development of Bio-Functionalized, Raman Responsive, and Potentially Excretable Gold Nanoclusters. *Nanomaterials* **2021**, *11*, 2181. [CrossRef]
76. Chen, X.Y.; Li, J.R.; Jiang, L. Two-dimensional arrangement of octadecylamine-functionalized gold nanoparticles using the LB technique. *Nanotechnology* **2000**, *11*, 108–111. [CrossRef]
77. Shellaiah, M.; Simon, T.; Sun, K.W.; Ko, F.-H. Simple bare gold nanoparticles for rapid colorimetric detection of Cr^{3+} ions in aqueous medium with real sample applications. *Sens. Actuators B Chem.* **2016**, *226*, 44–51. [CrossRef]
78. Brust, M.; Walker, M.; Bethell, D.; Schiffrin, D.J.; Whyman, R. Synthesis of thiol-derivatised gold nanoparticles in a two-phase Liquid–Liquid system. *J. Chem. Soc. Chem. Commun.* **1994**, 801–802. [CrossRef]
79. Briñas, R.P.; Maetani, M.; Barchi, J.J. A survey of place-exchange reaction for the preparation of water-soluble gold nanoparticles. *J. Colloid Interface Sci.* **2013**, *392*, 415–421. [CrossRef]
80. Dichello, G.A.; Fukuda, T.; Maekawa, T.; Whitby, R.L.D.; Mikhalovsky, S.V.; Alavijeh, M.; Pannala, A.S.; Sarker, D.K. Preparation of liposomes containing small gold nanoparticles using electrostatic interactions. *Eur. J. Pharm. Sci.* **2017**, *105*, 55–63. [CrossRef]
81. Praharaj, S.; Panigrahi, S.; Basu, S.; Pande, S.; Jana, S.; Ghosh, S.K.; Pal, T. Effect of bromide and chloride ions for the dissolution of colloidal gold. *J. Photochem. Photobiol. A Chem.* **2007**, *187*, 196–201. [CrossRef]
82. Kuroda, Y.; Fukumoto, K.; Kuroda, K. Uniform and high dispersion of gold nanoparticles on imogolite nanotubes and assembly into morphologically controlled materials. *Appl. Clay Sci.* **2012**, *55*, 10–17. [CrossRef]
83. Bastús, N.G.; Comenge, J.; Puntes, V. Kinetically Controlled Seeded Growth Synthesis of Citrate-Stabilized Gold Nanoparticles of up to 200 nm: Size Focusing versus Ostwald Ripening. *Langmuir* **2011**, *27*, 11098–11105. [CrossRef]
84. Ziegler, C.; Eychmüller, A. Seeded Growth Synthesis of Uniform Gold Nanoparticles with Diameters of 15−300 nm. *J. Phys. Chem. C* **2011**, *115*, 4502–4506. [CrossRef]

85. Zheng, Y.; Zhong, X.; Li, Z.; Xia, Y. Successive, Seed-Mediated Growth for the Synthesis of Single-Crystal Gold Nanospheres with Uniform Diameters Controlled in the Range of 5–150 nm. *Part. Part. Syst. Charact.* **2014**, *31*, 266–273. [CrossRef]
86. Oh, J.-H.; Sa, Y.-J.; Joo, S.-H.; Lee, J.-S. Assembling Gold Nanocubes Into a Nanoporous Gold Material. *Bull. Korean Chem. Soc.* **2012**, *33*, 1777–1780. [CrossRef]
87. Bhattarai, S.R.; Derry, P.J.; Aziz, K.; Singh, P.K.; Khoo, A.M.; Chadha, A.S.; Liopo, A.; Zubarev, E.R.; Krishnan, S. Gold nanotriangles: Scale up and X-ray radiosensitization effects in mice. *Nanoscale* **2017**, *9*, 5085–5093. [CrossRef] [PubMed]
88. Chateau, D.; Liotta, A.; Vadcard, F.; Navarro, J.R.G.; Chaput, F.; Lermé, J.; Lerouge, F.; Parola, S. From gold nanobipyramids to nanojavelins for a precise tuning of the plasmon resonance to the infrared wavelengths: Experimental and theoretical aspects. *Nanoscale* **2015**, *7*, 1934–1943. [CrossRef]
89. Khoury, C.G.; Vo-Dinh, T. Gold Nanostars For Surface-Enhanced Raman Scattering: Synthesis, Characterization and Optimization. *J. Phys. Chem. C* **2008**, *112*, 18849–18859. [CrossRef]
90. Nikoobakht, B.; El-Sayed, M.A. Preparation and Growth Mechanism of Gold Nanorods (NRs) Using Seed-Mediated Growth Method. *Chem. Mater.* **2003**, *15*, 1957–1962. [CrossRef]
91. Piella, J.; Bastús, N.G.; Puntes, V. Size-Controlled Synthesis of Sub-10-nanometer Citrate-Stabilized Gold Nanoparticles and Related Optical Properties. *Chem. Mater.* **2016**, *28*, 1066–1075. [CrossRef]
92. Cortez-Lemus, N.A.; Licea-Claverie, A.; Paraguay-Delgado, F.; Alonso-Nuñez, G. Gold Nanoparticles Size Design and Control by Poly(*N*,*N*′-diethylaminoethyl methacrylate). *J. Nanomater.* **2015**, *2015*, e273814. [CrossRef]
93. Xia, H.; Xiahou, Y.; Zhang, P.; Ding, W.; Wang, D. Revitalizing the Frens Method To Synthesize Uniform, Quasi-Spherical Gold Nanoparticles with Deliberately Regulated Sizes from 2 to 330 nm. *Langmuir* **2016**, *32*, 5870–5880. [CrossRef]
94. Liu, J.; Yu, M.; Zhou, C.; Yang, S.; Ning, X.; Zheng, J. Passive Tumor Targeting of Renal-Clearable Luminescent Gold Nanoparticles: Long Tumor Retention and Fast Normal Tissue Clearance. *J. Am. Chem. Soc.* **2013**, *135*, 4978–4981. [CrossRef]
95. Yu, M.; Zhou, C.; Liu, L.; Zhang, S.; Sun, S.; Hankins, J.D.; Sun, X.; Zheng, J. Interactions of Renal-Clearable Gold Nanoparticles with Tumor Microenvironments: Vasculature and Acidity Effects. *Angew. Chem. Int. Ed.* **2017**, *56*, 4314–4319. [CrossRef]
96. Xi, W.; Haes, A.J. Elucidation of HEPES Affinity to and Structure on Gold Nanostars. *J. Am. Chem. Soc.* **2019**, *141*, 4034–4042. [CrossRef] [PubMed]
97. Yang, Y.; Serrano, L.A.; Guldin, S. A Versatile AuNP Synthetic Platform for Decoupled Control of Size and Surface Composition. *Langmuir* **2018**, *34*, 6820–6826. [CrossRef]
98. Wu, B.-H.; Yang, H.-Y.; Huang, H.-Q.; Chen, G.-X.; Zheng, N.-F. Solvent effect on the synthesis of monodisperse amine-capped Au nanoparticles. *Chin. Chem. Lett.* **2013**, *24*, 457–462. [CrossRef]
99. Liu, J.; Yu, M.; Ning, X.; Zhou, C.; Yang, S.; Zheng, J. PEGylation and Zwitterionization: Pros and Cons in the Renal Clearance and Tumor Targeting of Near-IR-Emitting Gold Nanoparticles. *Angew. Chem. Int. Ed.* **2013**, *52*, 12572–12576. [CrossRef] [PubMed]
100. Choi, H.S.; Liu, W.; Misra, P.; Tanaka, E.; Zimmer, J.P.; Ipe, B.I.; Bawendi, M.G.; Frangioni, J.V. Renal clearance of quantum dots. *Nat. Biotechnol.* **2007**, *25*, 1165–1170. [CrossRef] [PubMed]
101. *Advances in Nanotheranostics, I.*; Springer: New York, NY, USA, 2015; ISBN 978-3-662-48542-2.
102. Patra, J.K.; Das, G.; Fraceto, L.F.; Campos, E.V.R.; del Pilar Rodriguez-Torres, M.; Acosta-Torres, L.S.; Diaz-Torres, L.A.; Grillo, R.; Swamy, M.K.; Sharma, S.; et al. Nano based drug delivery systems: Recent developments and future prospects. *J. Nanobiotechnol.* **2018**, *16*, 71. [CrossRef]
103. Duan, X.; Li, Y. Physicochemical Characteristics of Nanoparticles Affect Circulation, Biodistribution, Cellular Internalization, and Trafficking. *Small* **2013**, *9*, 1521–1532. [CrossRef]
104. Kim, H.; Lee, D. Near-Infrared-Responsive Cancer Photothermal and Photodynamic Therapy Using Gold Nanoparticles. *Polymers* **2018**, *10*, 961. [CrossRef]
105. Le, K.Q.; Alù, A.; Bai, J. Multiple Fano interferences in a plasmonic metamolecule consisting of asymmetric metallic nanodimers. *J. Appl. Phys.* **2015**, *117*, 023118. [CrossRef]
106. Martínez, Á.; Lyu, Y.; Mancin, F.; Scrimin, P. Glucosamine Phosphate Induces AuNPs Aggregation and Fusion into Easily Functionalizable Nanowires. *Nanomaterials* **2019**, *9*, 622. [CrossRef] [PubMed]
107. Rengan, A.K.; Bukhari, A.B.; Pradhan, A.; Malhotra, R.; Banerjee, R.; Srivastava, R.; De, A. In Vivo Analysis of Biodegradable Liposome Gold Nanoparticles as Efficient Agents for Photothermal Therapy of Cancer. *Nano Lett.* **2015**, *15*, 842–848. [CrossRef] [PubMed]
108. Chou, L.Y.T.; Zagorovsky, K.; Chan, W.C.W. DNA assembly of nanoparticle superstructures for controlled biological delivery and elimination. *Nat. Nanotechnol.* **2014**, *9*, 148–155. [CrossRef] [PubMed]
109. Mapanao, A.K.; Santi, M.; Faraci, P.; Cappello, V.; Cassano, D.; Voliani, V. Endogenously Triggerable Ultrasmall-in-Nano Architectures: Targeting Assessment on 3D Pancreatic Carcinoma Spheroids. *ACS Omega* **2018**, *3*, 11796–11801. [CrossRef] [PubMed]
110. Cassano, D.; Summa, M.; Pocoví-Martínez, S.; Mapanao, A.-K.; Catelani, T.; Bertorelli, R.; Voliani, V. Biodegradable Ultrasmall-in-Nano Gold Architectures: Mid-Period In Vivo Distribution and Excretion Assessment. *Part. Part. Syst. Charact.* **2019**, *36*, 1800464. [CrossRef]
111. Katrina Mapanao, A.; Giannone, G.; Summa, M.; Laura Ermini, M.; Zamborlin, A.; Santi, M.; Cassano, D.; Bertorelli, R.; Voliani, V. Biokinetics and clearance of inhaled gold ultrasmall-in-nano architectures. *Nanoscale Adv.* **2020**, *2*, 3815–3820. [CrossRef]

112. Santi, M.; Mapanao, A.K.; Cassano, D.; Vlamidis, Y.; Cappello, V.; Voliani, V. Endogenously-Activated Ultrasmall-in-Nano Therapeutics: Assessment on 3D Head and Neck Squamous Cell Carcinomas. *Cancers* **2020**, *12*, 1063. [CrossRef]
113. Mapanao, A.K.; Santi, M.; Voliani, V. Combined chemo-photothermal treatment of three-dimensional head and neck squamous cell carcinomas by gold nano-architectures. *J. Colloid Interface Sci.* **2021**, *582*, 1003–1011. [CrossRef]
114. Cassano, D.; Santi, M.; D'Autilia, F.; Mapanao, A.K.; Luin, S.; Voliani, V. Photothermal effect by NIR-responsive excretable ultrasmall-in-nano architectures. *Mater. Horiz.* **2019**, *6*, 531–537. [CrossRef]
115. Higbee-Dempsey, E.M.; Amirshaghaghi, A.; Case, M.J.; Bouché, M.; Kim, J.; Cormode, D.P.; Tsourkas, A. Biodegradable Gold Nanoclusters with Improved Excretion Due to pH-Triggered Hydrophobic-to-Hydrophilic Transition. *J. Am. Chem. Soc.* **2020**, *142*, 7783–7794. [CrossRef]
116. Cheheltani, R.; Ezzibdeh, R.M.; Chhour, P.; Pulaparthi, K.; Kim, J.; Jurcova, M.; Hsu, J.C.; Blundell, C.; Litt, H.I.; Ferrari, V.A.; et al. Tunable, biodegradable gold nanoparticles as contrast agents for computed tomography and photoacoustic imaging. *Biomaterials* **2016**, *102*, 87–97. [CrossRef] [PubMed]
117. Yahia-Ammar, A.; Sierra, D.; Mérola, F.; Hildebrandt, N.; Le Guével, X. Self-Assembled Gold Nanoclusters for Bright Fluorescence Imaging and Enhanced Drug Delivery. *ACS Nano* **2016**, *10*, 2591–2599. [CrossRef] [PubMed]
118. Tam, J.M.; Tam, J.O.; Murthy, A.; Ingram, D.R.; Ma, L.L.; Travis, K.; Johnston, K.P.; Sokolov, K.V. Controlled Assembly of Biodegradable Plasmonic Nanoclusters for Near-Infrared Imaging and Therapeutic Applications. *ACS Nano* **2010**, *4*, 2178–2184. [CrossRef] [PubMed]
119. Deng, H.; Dai, F.; Ma, G.; Zhang, X. Theranostic Gold Nanomicelles made from Biocompatible Comb-like Polymers for Thermochemotherapy and Multifunctional Imaging with Rapid Clearance. *Adv. Mater.* **2015**, *27*, 3645–3653. [CrossRef] [PubMed]